Vehicle Level Tip-to-Tail Modeling of an Aircraft

Rory A. Roberts[1] and Scott M. Eastbourn

Wright State University, Dayton OH 45435
E-mail: [1]rory.roberts@wright.edu

Abstract

A system-level multidisciplinary aircraft model has been developed exclusively in MATLAB/Simulink. Aircraft subsystem models representing the air vehicle system, propulsion system, robust electrical power system, thermal management systems, actuation system and their associated controllers were integrated to investigate the thermal management issues of a long range strike platform. The aircraft model coined tip-to-tail modeling and simulation tool (T2T M&S) allows conceptual design trade studies of various subsystems and can quantify performance gains across the aircraft. As a result, the thermal and power challenges that face modern aircraft can be addressed, potentially increasing the performance capabilities of future aircraft. Preliminary simulation results are discussed with a specific focus on thermal management during mission segments of high thermal demands.

Keywords: Energy optimization; tip-to-tail; aircraft model; thermal management; dynamic model; engine model.

1. Introduction

Future aircraft will face an escalating number of energy and thermal challenges. Aircraft are utilizing more-electric components and require an increase in power generation as a result. In fact, the power system demands have grown by nearly an order of magnitude to support these new high-power loads, increasing the internal heat generated by the aircraft that must be removed by the thermal management system (TMS) [1]. Future aircraft will have power and thermal demands increase an additional order of magnitude to support advanced electronic systems [2]. Simultaneously, restrictions have significantly been imposed to the thermal management system. Modern aircraft must maintain low radar observability and infra-red signature [3]. For example, the ram air heat exchanger inlet areas have been greatly condensed or eliminated, reducing the effectiveness of a vital heat sink. In addition, new composite aircraft skins have reduced the amount of heat that can be rejected to the environment. The combination of these characteristics has increased the challenges faced by modern TMSs. In order to assist in the mitigation of these thermal challenges, new modeling and simulation tools need to be developed [4].

Aircraft in the conceptual stage have traditionally been designed at the subsystem-level. These subsystems, such as the propulsion, electrical, and thermal management, systems are often designed and optimized without consideration of vehicle-level interactions among the other subsystems. As a result, the final aircraft design may not truly be optimized. Vehicle-level analysis of subsystem interactions could result in significant performance gains across the aircraft, potentially improving the overall effectiveness of future platforms. The development of a modeling and simulation (M&S) tool allows these performance gains to be quantified.

Work has been performed for hybrid electric vehicles for design and performance optimization. Models are evaluated for their accuracy in capturing the dynamic behavior of the electrical subsystems [5]. A vehicle level model has also been developed for exergetic, exergoeconomic and exergoenvironmental optimization for hybrid electric vehicle [6]. The vehicle level model provided the ability to optimize multiple objectives simultaneously.

Tip-to-tail efforts have already been conducted [7]–[9]. Many of these models, however, were primarily steady-state and lacked important dynamic effects or contained proprietary subsystem models. Work by Airbus has proposed techniques based on the system identification theory which consists on heuristically determining an analytical model using physical insights and measurements [10]. The current work has developed a new modeling tool without proprietary data and exclusively in MATLAB/Simulink. In addition, special attention is paid to capture transient behaviors, including the Integrated Power Package (IPP), heat exchangers, fuel and oil pumps, and engine oil heat rejection. The vehicle-level model, named the tip-to-tail modeling and simulation tool (T2T M&S) was developed by integrating various aircraft subsystems.

2. Tip-to-Tail Model Development

A vehicle-level aircraft model has been developed in a multidisciplinary modeling and simulation environment. Individual subsystem models were developed in a MATLAB/Simulink environment to investigate a notional long range strike platform.

Figure 1 shows a Simulink screenshot of the vehicle-level model. The T2T M&S is divided into five subsystems: Aircraft Vehicle System (AVS), Engine, Adaptive Power and Thermal Management System (APTMS), Fuel Thermal Management System (FTMS), High Power Electric Actuation System (HPEAS) and Robust Electrical Power System (REPS). More detail is provided in the following sections.
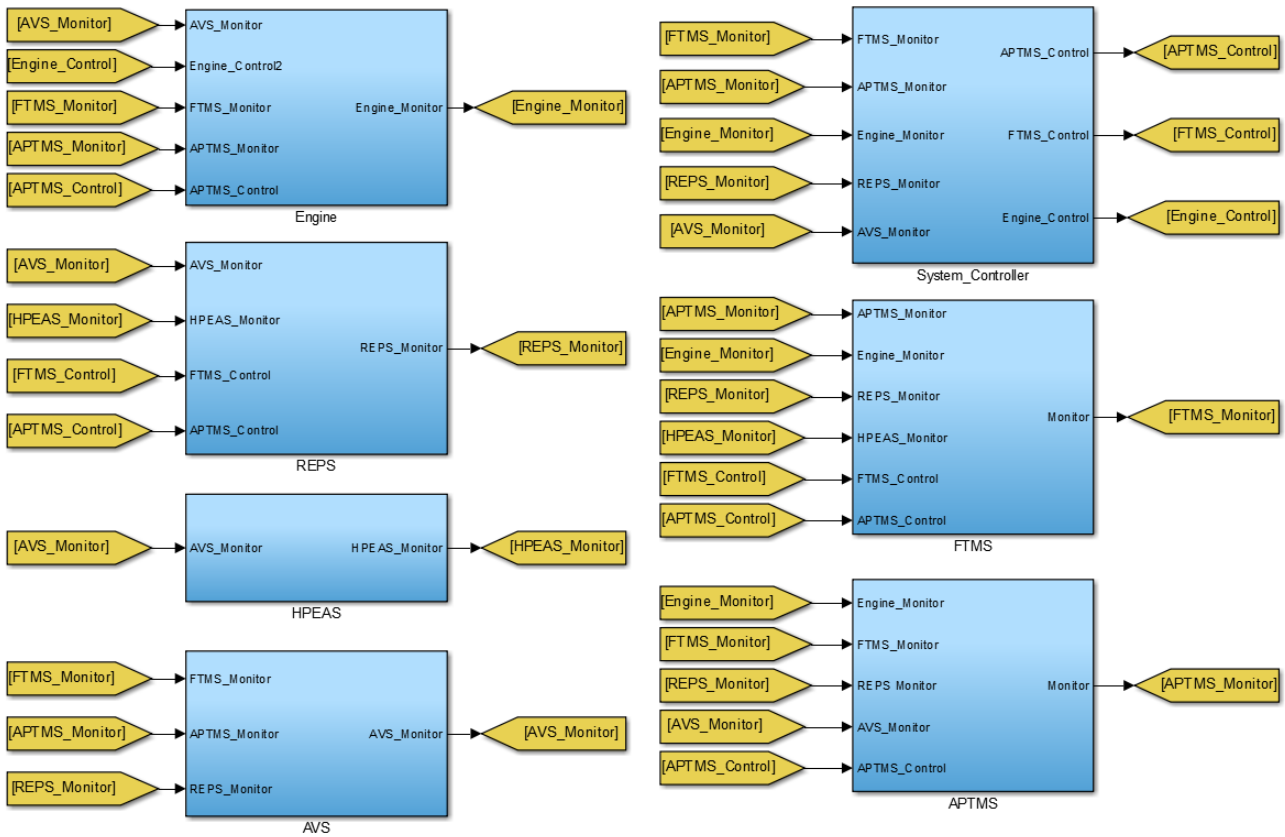

**Corresponding Author

Figure 1. System-Level Simulink Model with Air Vehicle System (AVS), Advanced Power and Thermal System (APTMS), Engine, Fuel Thermal Management System (FTMS), High Power Electrical Actuation System (HPEAS), Robust Electrical Power System (RPS) and System Controller.
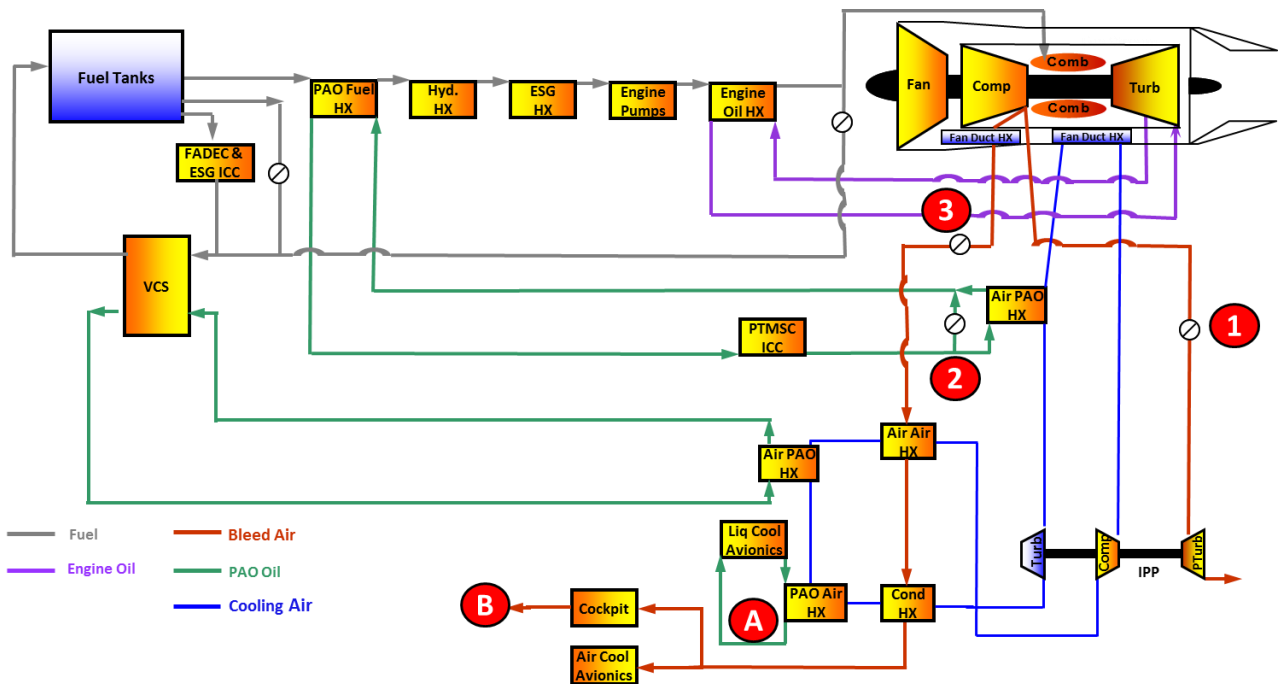

Figure 2. Adaptive Power and Fuel Thermal Management System with FADEC and generator controller heat load (FADEC & ESG ICC), vapor cycle system (VCS), Polyalphaolefin oil and fuel heat exchanger (PAO Fuel HX), hydraulics heat exchanger (HYD. HX), electric generator heat exchanger (ESG HX), fuel pump heat load (Engine pumps), engine oil heat exchanger (Engine Oil HX), fan duct heat exchangers (Fan Duct HX), thermal management system controller heat load (PTMSC ICC), air and Polyalphaolefin oil heat exchanger (Air PAO HX), recuperator heat exchanger (Air Air HX), Liquid cooled avionics load (Liq Cool Avionics), Polyalphaolefin oil and air heat exchanger (PAO Air HX), conditioning heat exchanger (Cond HX), closed-loop turbine (Turb), closed-loop compressor (Comp), power turbine (PTurb), integrated power package (IPP) and valves 1,2 and 3.

Figure 3. Turbofan engine diagram with fan, compressor, turbines, shafts, bypass, heat exchanger, nozzle and combustor.

2.1 Aircraft Vehicle System

The first subsystem is the Aircraft Vehicle System (AVS) model. The AVS model contains the mission profile data as well as the forces acting on the aircraft, such as weight, drag, thrust and lift. The mission profile consists of predefined waypoints for Mach number and altitude at various mission times. The AVS model calculates a required thrust to maintain the desired mission profile and relays this thrust to the engine model. The AVS model has two options for modeling the physics of the air vehicle. The first option for the AVS model offers all six degrees of freedom (6 DoF) with translational and rotational axis. The 6 DoF model provides aircraft position, velocity, and orientation. The 6 DoF includes flight controls and the ability to integrate directly with actuators and control surfaces [7]. The second option is drag-polar model that only provides the drag and lift forces. In this work, the drag polar model is used.

The drag polar model is a steady-state representation of the balanced forces acting on the aircraft. The force of lift as it relates to aircraft velocity is provided in Eq. (1). In steady conditions the force of lift is equal to the weight of the aircraft. The drag force is found using Eq. (2) with relation to the aircraft velocity. In steady conditions the force of drag is equal the thrust. During simulation, the weight of the aircraft along with the aircraft speed, U_{ac}, are used to calculate the lift coefficient, C_L. The lift coefficient is then used to calculate the drag coefficient, C_D using Eq. (3). From Eq. (2), the required thrust is calculated using C_D and the aircraft velocity. The coefficients C_{D0} and C_{L0} are unique to the aircraft platform and design.

$$F_L = \frac{1}{2}\rho_{atm}U_{ac}^2 SC_L = Weight \qquad (1)$$

$$F_D = \frac{1}{2}\rho_{atm}U_{ac}^2 SC_D = Thrust \qquad (2)$$

$$C_D = C_{D0} + C_{D1}(C_L - C_{L0})^2 \qquad (3)$$

2.2 Engine

The aircraft in this effort utilizes two engines, each producing a maximum sea-level standard thrust of 89 kN to meet the thrust demands of the mission. The engine controller (FADEC) alters the fuel flow to the engine in order to produce the thrust demanded by the AVS model (autopilot). The engine model also interacts with the vehicle's TMS, which is divided into two parts: the APTMS and the FTMS. Both the APTMS and FTMS shown in Figure 2 are provided in more detail in following sections.

The engine model captures the shaft and plenum volume dynamics.

Figure 3 presents a detailed diagram of all the components modeled and captured within the engine model. The model components are: fan, compressor bypass, low pressure and high pressure shafts, combustor, low pressure and high pressure turbines, fan duct/bypass heat exchangers and nozzle. More detail on the engine model is found in previous work [11,12].
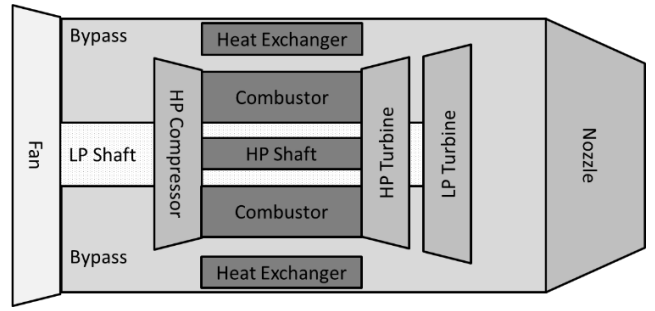
2.3 Adaptive Power and Thermal Management System

The Adaptive Power and Fuel Thermal Management System (APTMS) is presented in Figure 2 (FTMS also). The APTMS model contains the Integrated Power Package (IPP), an air cycle machine that cools the cockpit, air-cooled avionics, and liquid-cooled avionics. A majority of the thermal loads within the APTMS ultimately reject heat to the engine bypass in the fan duct through the fan duct heat exchanger (HX). The remaining APTMS heat loads are transferred to the FTMS via the Air-PAO HX and are ultimately rejected to the fuel (valve 2).

IPP

The IPP model, shown in Figure 4, is the prime mover of thermal energy in the APTMS. The IPP is responsible for cooling the air cooled avionics, cockpit, and liquid cooled avionics. The IPP consists of a power turbine, closed loop compressor, and closed loop turbine. The IPP extracts high pressure bleed air from the engine compressor to the power turbine for additional shaft work. The IPP can operate in constant angular shaft speed mode or variable shaft speed mode.

In order to capture dynamics within the IPP model, two different approaches are employed. First, an intercomponent volume method is used by modeling a plenum volume before each of the different turbomachinery models. In the case of the IPP, plenum volumes are placed before the power turbine, closed loop compressor, and closed loop turbine as shown simplified in Figure 4. The plenum volumes are isentropic ducts with the velocity low enough to assume zero momentum variations [13]. The dynamic pressure of the plenum volume can be calculated assuming a perfect gas, as shown by Eq.(4).
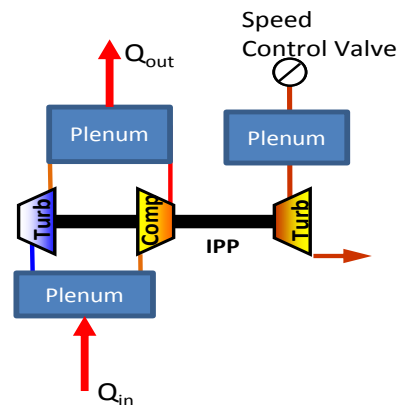

Figure 4. Simplified diagram of integrated power package (IPP) with plenum volumes, compressor, turbines and speed control valve.

$$P = \int \frac{(\dot{m}_{in} - \dot{m}_{out})RT}{V} dt \qquad (4)$$

The turbomachinery models contain generic performance maps that can easily be based on experimental data. These maps are a function of shaft speed, pressure ratio, and inlet conditions, such as temperature, pressure and molar composition of the incoming air, and output a corrected mass flow. The turbomachinery mass flows are used for the incoming and outgoing mass flows in Eq.(4) for the plenum volumes.

The maps are represented by two-dimensional lookup tables that contain a predetermined matrix for the specific turbo-machine being used. Row and column vectors are also defined within the map, allowing interpolation within the matrix based on the input signals to the lookup table. These input signals are normalized speeds and pressure ratio, shown below by Eq. (5) and Eq. (6) respectively. Using these two normalized signals, the performance map interpolates within the predefined matrix an output of a normalized mass flow rate. This normalized mass flow rate is used to calculate an actual mass flow rate using Eq. (7).

$$P_{r\_normalized} = \frac{P_{out}}{P_{in}P_{r,design}} \qquad (5)$$

$$N_{normalized} = \left(\frac{N_{shaft}}{\sqrt{T_{in}}}\right)\left(\frac{\sqrt{T_{in,design}}}{N_{design}}\right) \qquad (6)$$

$$\dot{m}_{actual} = \dot{m}_{normalized}\left(\frac{\dot{m}_{design}\sqrt{T_{in,design}}}{P_{in,design}}\right)\left(\sqrt{\frac{P_{in}}{T_{in}}}\right) \qquad (7)$$

Each turbo-machinery component model contains a performance map that determines an efficiency for a given shaft speed and pressure ratio. Just as the mass flow rate performance map, the efficiency performance map contains a matrix defining efficiencies for predetermined shaft speeds and pressure ratios. The normalized signals for pressure ratio and shaft speed are shown in Eq. (5) and Eq. (6) respectively. The efficiency term yielded from the performance map is then used to calculate the outlet temperature for the compressor and turbine models, shown by Eq. (8) and Eq. (9) respectively.

$$T_{out,comp} = T_{in}\left(1 + \frac{1}{\eta}\frac{P_{out}}{P_{in}}\right)^{\left(\frac{\gamma-1}{\gamma}-1\right)} \qquad (8)$$

$$T_{out,turb} = T_{in}\left(1 + \eta\frac{P_{in}}{P_{out}}\right)^{\left(\frac{\gamma-1}{\gamma}-1\right)} \qquad (9)$$

The work absorbed or produced is based on the outlet mass flow rates as well as the inlet and outlet temperatures for each of the turbo-machine models. The compressor model produces negative work while the turbines produce positive work. The inlet and outlet temperatures of each model are used to calculate an enthalpy value. These inlet and outlet enthalpies are combined with the outlet mass flow rate to calculate the work for the compressor and turbine models, as shown by Eq. (10) and Eq. (11) respectively.

$$\dot{W}_{comp} = \dot{m}_{actual}(h_{in} - h_{out}) \qquad (10)$$

$$\dot{W}_{turb} = \dot{m}_{actual}(h_{in} - h_{out}) \qquad (11)$$

Secondly, the IPP model considers shaft inertia. Any changes in torque to the IPP shaft will vary the shaft speed. By considering the shaft inertia, however, this variation does not occur instantaneously. This time delay is captured by Eq. (12).

$$N = \frac{30}{\pi} \int \frac{\dot{W}_{Power,turb} + \dot{W}_{CL,turb} + \dot{W}_{CL,comp}}{J_{shaft}\omega_{shaft}} \qquad (12)$$

The IPP speed control valve, labeled valve 1 in Figure 2, is located between the IPP power turbine and the main engine compressor. The IPP speed control valve regulates the mass flow of high pressure bleed air from the engine compressor to the power turbine. The control valve is modeled as a variable area orifice and the model calculates the mass flow based Eq. (13), assuming non-choked flow. The Mach number, density and temperature at the throat are calculated using Eqs. (14), (15) and (16), respectively. For choked flow, the mass flow is calculated using Eq. (17).

$$\dot{m}_{CV} = A_{th}Ma\rho_{th}\sqrt{\left(\frac{RT_{th}\gamma}{MW}\right)} \qquad (13)$$

$$Ma = \sqrt{\left(\frac{2}{\gamma-1}\right)\left[\left(\frac{P_{in}}{P_{out}}\right)^{\left(\frac{\gamma-1}{\gamma}\right)} - 1\right]} \qquad (14)$$

$$\rho_{th} = \rho\left(\frac{1}{1+\frac{\gamma-1}{2}Ma^2}\right)^{\frac{1}{\gamma-1}} \qquad (15)$$

$$T_{th} = T_{in}\left(\frac{1}{1+\frac{\gamma-1}{2}Ma^2}\right) \qquad (16)$$

$$\dot{m}_{CV} = P_{in}A_{th}\sqrt{\frac{\gamma}{RT_{in}}}\left(\frac{2}{\gamma+1}\right)^{\left(\frac{\gamma+1}{2(\gamma-1)}\right)} \qquad (17)$$

The IPP speed control valve is operated to maintain a POA oil temperature of 20°C in the liquid cooled avionics loop (Point A, Figure 2). A PI controller calculates the error between the liquid cooled avionics temperature and the set point value of 20°C, and then adjusts the IPP speed control valve accordingly until the error is zero. The results will be shown later for the control valve response.

Heat Exchangers

The heat exchanger models from previous efforts were used [11,14]. A counter-flow, plate-fin heat exchanger is assumed. The heat exchanger models account for the volume and mass of the heat exchanger component and impact the aircraft's total mass. The heat exchanger material is considered, as the heat exchanger mass stores and supplies thermal energy depending on the perturbation. In this effort, the heat exchangers are divided into three separate nodes and are assumed constructed out of aluminum. These nodes allow the user to obtain more detailed temperature distributions through the heat exchanger material as well as create a counter flow heat exchanger. The energy balance calculations completed in each of the fluid streams are shown in Eqs. (18) to (21). The heat exchanger material block computes an energy balance using Eq. (18) and relays the heat exchanger temperature to the fluid stream blocks. Eqs. (19) and (20) provide the energy balance for calculation of the temperatures for each flow stream. The heat flows, Q, are calculated using Eq. (21)

$$m_{HX} c_{v,HX} \frac{dT_{HX}}{dt} = \dot{Q}_{cold} + \dot{Q}_{hot} \tag{18}$$

$$m_{hot} c_{v,hot} \frac{dT_{cold}}{dt} = \dot{Q}_{hot} + \dot{m}_{hot} h_{hot,in} - \dot{m}_{hot} h_{hot,out} \tag{19}$$

$$m_{cold} c_{v,cold} \frac{dT_{cold}}{dt} = \dot{Q}_{cold} + \dot{m}_{cold} h_{cold,in} - \dot{m}_{cold} h_{cold,out} \tag{20}$$

$$\dot{Q}_i = h_c A_{HX} (T_{fluid} - T_{HX}) \tag{21}$$

For additional detail, the heat transfer coefficient, h_c, shown in Eq. (21) is fluid and flow dependent. Using physical parameters specified by the user, the Reynolds number is calculated for each stream and node. The Nusselt number is calculated using the Gnielinski Correlations, Eqs. (22) through (24) [15]. The convective heat transfer coefficient is then derived using the thermal conductivity and hydraulic diameter of the heat exchanger channels, as shown by Eq. (25).

$$Nu = \frac{(f/2)(Re-1000) Pr}{1+12.7(f/2)(Pr^{2/3}-1)} \left[1 + \left(\frac{D_h}{L} \right)^{2/3} \right]$$
$$Re = [2300, 5*10^4] \tag{22}$$
$$Pr = [0.5, 2000]$$

$$Nu = 0.0214(Re^{0.8} - 100) Pr^{0.4} \left[1 + \left(\frac{D_h}{L} \right)^{2/3} \right]$$
$$Re = [10^4, 5*10^6] \tag{23}$$
$$Pr = [0.5, 1.5]$$

$$Nu = 0.012(Re^{0.87} - 280) Pr^{0.4} \left[1 + \left(\frac{D_h}{L} \right)^{2/3} \right]$$
$$Re = [3*10^3, 10^6] \tag{24}$$
$$Pr = [1.5, 500]$$

$$h_c = Nu \left(\frac{k_f}{D_h} \right) \tag{25}$$

2.4 Fuel Thermal Management System

The FTMS model removes heat from the generator, actuators, FADEC, PTMSC ICC, ESG ICC, engine oil, oil pumps, and fuel pumps. Models were developed for the oil and fuel pumps, capturing the time-variant heat rejection from each pump. The FTMS also contains dynamic models for the engine oil heat rejection.

Fuel and Oil Pumps

A quasi-steady-state pump model has been developed (the pump inertia is not considered). This model is used for both the engine fuel and oil pumps. The pump designs are currently defined with a design mass flow and design pressure ratio, which dictates the reversible work rate at design point. The efficiency is used to determine the actual work rate with relation to the reversible rate. The model is designed so that pump speed is directly related to engine speed through an assumed constant gear ratio. This provides off-design operation by operating the pump at various speeds. In addition, the pump work rate also leads to the generation of heat that is then rejected to the fluid stream. The TMS is designed to dissipate these time-variant heat loads. In fact, the pumps are a significant heat source for the FTMS loops.

The performance characteristics of these pumps are represented by generic maps stored in a spreadsheet. This simplification is sufficient for determining the transient heat loads of the pumps throughout the mission and is the standard industry approach. This data can be populated with experimental pump data by the user. These maps contain mass flow rate data as a function of pressure ratio and rotation speed as shown in Eq. (26).

$$\dot{m}_{pump} = f\left(\frac{P_{out}}{P_{in}}, N_{shaft} \right) \tag{26}$$

This mass flow is used to calculate the pump work using Eq. (27). The fluid temperature rise is the computed using the energy balance of Eq.(28)[16].

$$\dot{W}_{pump} = \dot{m}_{pump} \frac{(P_{out} - P_{in})}{\eta_{pump} \rho_{fluid}} \tag{27}$$

$$T_{out} = \frac{\dot{W}_{pump}}{\dot{m}_{pump} c_{p,oil}} + T_{in} \tag{28}$$

Engine Oil Heat Rejection

Similarly to the fuel and oil pumps, the heat rejected directly from the engine to the oil can be significant. The engine oil heat load is physically modeled in this effort. This is done by creating an oil loop that interacts with four heat transfer nodes representing the engine fan, compressor,

low-pressure turbine, and high-pressure turbine shaft bearings. The oil loop absorbs heat from each of these bearings in parallel and then transfers this heat to the fuel stream through an additional heat exchanger.

The heat transfer at each of these four nodes is determined with Eq. (29) using the temperature difference between the oil and the bearing node. The temperature data at each engine station comes directly from the engine model.

$$\dot{Q}_{node} = \frac{(T_{node} - T_{out,oil})}{R_T} \qquad (29)$$

This thermal resistance, R_T, is estimated using design point data consisting of the engine temperatures, temperature rise of the oil and mass flow of the oil as shown in Eq. (30).

$$R_T = \left(\frac{(T_{node} - T_{out,oil})}{\dot{m}_{oil} c_{p,oil}(T_{out,oil} - T_{in,oil})} \right)_{Design} \qquad (30)$$

APTMS Heat Rejection to Fuel

The APTMS rejects heat to the FTMS fuel stream via valve 2 in Figure 2. The APTMS and FTMS are thermally connected by a PAO oil loop. As additional heat rejection is needed by the APTMS, valve 2 will begin to shut sending a larger percentage of the PAO oil through the Air-PAO HX in Figure 2. When valve 2 is fully open, 20% of the PAO oil passes through the heat exchanger while 80% is bypassed. When valve 2 is fully closed, 100% of the PAO oil passes through the heat exchanger.

2.5 High Power Electric Actuation System and Robust Electrical Power System

The HPEAS are solely modeled from a thermal standpoint and include the actuators. The only contributions from this system is predefined heat loads, which are a function of mission time.

The REPS has an electrical bus with all the major electrical equipment represented by simple models. REPS components include the generator, and avionics, controllers, IPP motor/generator and advanced electronic weapon heat loads. The electrical equipment assumes a constant electrical efficiency.

3. Simulation Results

The aircraft tip-to-tail model is simulated in Simulink using the mission profile illustrated in Figure 5. The mission profile consist of a two hour mission with varying altitude and Mach number. The aircraft performs a high altitude cruise with low altitude loiter followed by a mid-altitude return.

The heat loads vary throughout the mission dependent on aircraft speed, altitude, engine throttle and electrical demands. Figure 6 presents the heat loads for the REPS and HPEAS. The REPS heat load is the summation of the air cooled avionics, liquid cooled avionics, FADEC ICC, PTMSC ICC, generator (ESG) and cockpit. The HPEAS heat load is currently a constant heat load produced by the actuators.
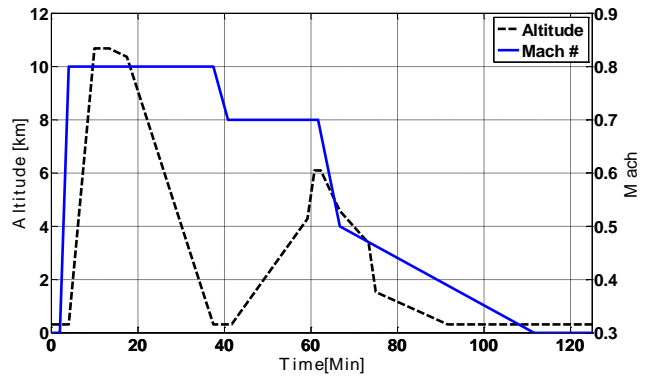

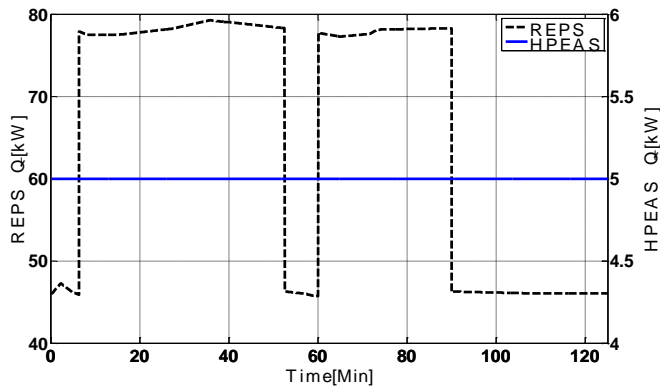Figure 5. Aircraft mission profile used for simulation. Both altitude and Mach # are presented.

Figure 6. Aircraft heat loads used for simulation. The heat loads for the REPS consist: air cooled avionics, liquid cooled avionics, FADEC ICC, PTMSC ICC, generator (ESG) and cockpit. The HPEAS heat loads consist of the actuator heat loads

The oil cooler removes heat from the engine oil through a oil-to-fuel heat exchanger. The heat rejected is presented in *Figure* 7. The total heat rejected is for two engines operating identically.
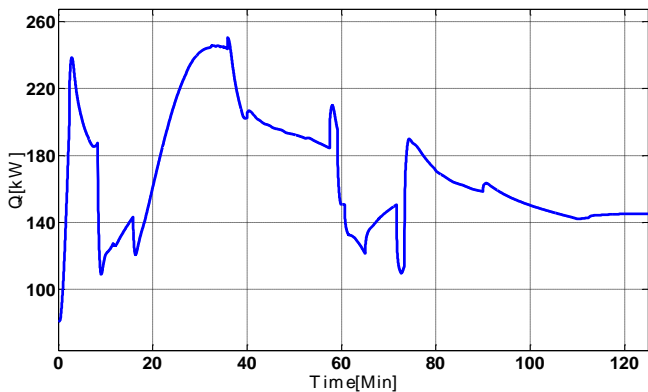

Figure 7. The heat load for the engine oil cooler. The heat load, $\dot{Q}$, from all nodes in Eq. (29) is presented.

As previously discussed, the AVS model calculates a required thrust based on the desired Mach number and altitude. This demanded thrust is sent to the engine controller which alters the fuel flow to produce the needed thrust. Notice the large and rapid descents of the aircraft at mission times of approximately 20 min. and 70 min.

Figure 8 illustrates the demanded thrust compared to the actual thrust. It is worth noting that the actual thrust saturates at 70 min. to a value of 0 lb. The mission time

corresponds to the rapid descent in the aircraft altitude and speed. In order to prevent the aircraft from exceeding the specified Mach number, the demanded engine thrust becomes negative. To prevent the engine controller from attempting to produce a negative thrust, a saturation limit of 0 lb. is placed on the engine thrust.
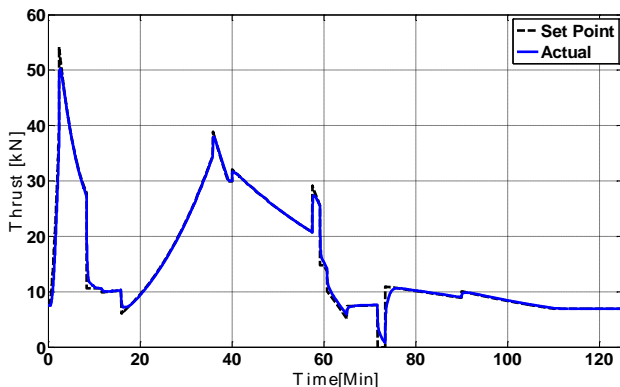

Figure 8. Aircraft actual and demanded thrust profiles. The set point thrust is determined by the AVS. The actual thrust is solved by the engine model.

As previously mentioned, key parameters are tracked throughout the mission. These temperatures, control valve positions, flow rates, and pressures are plotted in order to determine the effectiveness of the FTMS and APTMS subsystems. Temperatures in particular are compared to previously determined limits in order to show compliance as the mission progresses. These results are summarized here.

Figure 9 and Figure 10 display two different plots related to the IPP. The first plot compares the actual and demanded IPP rotational speeds, while the second plot illustrates the actual mass flow to the IPP power turbine along with the corresponding control valve position.

Figure 11 shows the liquid cooled avionics (LCA) temperature profile along with its controller set point. The desired set point temperature for the oil entering the liquid cooled avionics heat exchanger is 20 °C, represented by the dashed line.
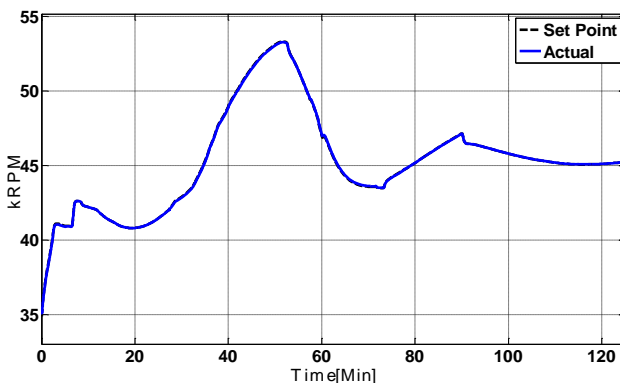

Figure 9. IPP Rotational Speed Profile. Both set point speed from thermal management controller and the actual speed are presented. The actual speed follows the set point very closely, making it difficult to see the set point dashed line.
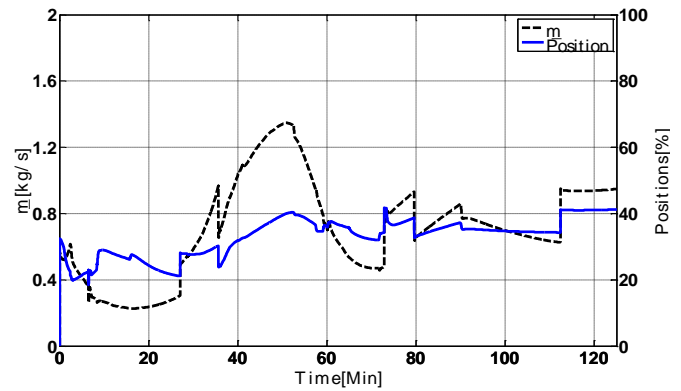

Figure 10. IPP speed control valve profile. The bleed mass flow, ṁ, for the IPP power turbine is presented along with the speed control valve position which controls the mass flow.
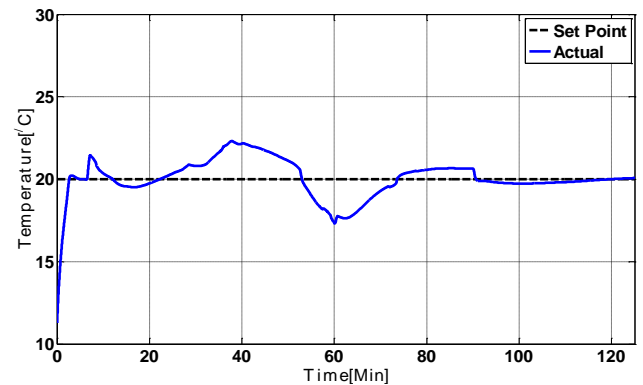

Figure 11. Liquid cooled avionic temperature throughout the mission.

As shown in Figure 11, the LCA temperature was controlled closely to the set-point temperature. The IPP speed in Figure 9 varies between 35,000 RPM and 55,000 RPM approximately during the mission in order to maintain the LCA temperature. The corresponding mass flow in Figure 10 for the IPP power turbine is regulated to achieve the IPP RPM set point.

Around 30 minutes into the mission, the IPP becomes more aggressive in controlling the LCA temperature. There are sharp changes in the IPP speed control valve in Figure 10 in reaction to the climbing LCA temperature. The FTMS heat exchanger bypass control valve in Figure 12 also begins to close when the LCA temperature continues to increase to provide additional cooling by dumping heat to the engine fuel.

Finally, the temperature and mass of fuel in the fuel tanks are shown in Figure 13. The total fuel mass has a relatively constant reduction rate as fuel is burned, while the temperature increases. The fuel temperature increases for the duration of the mission. It is important to note that this fuel temperature must be controlled in order to prevent coking and to ensure sufficient component cooling. The fuel temperature is maintained below 60 °C, which well below the coking limits of the fuel.
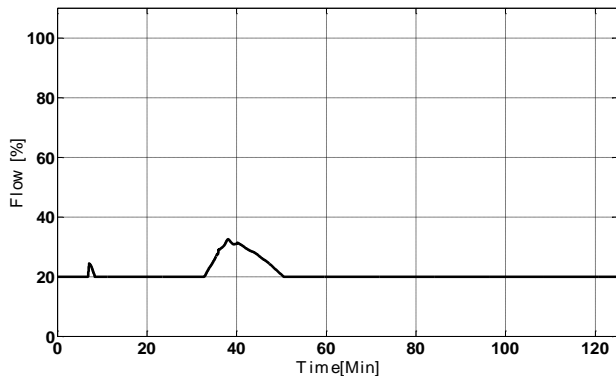
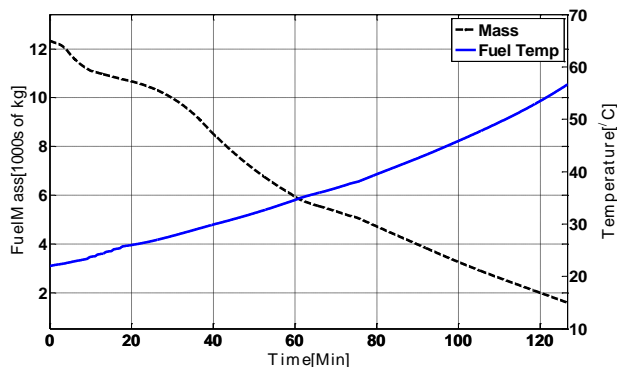*Figure 12. FTMS heat exchanger bypass control valve profile.*

Figure 13. Fuel variation throughout mission. The total mass of fuel decreases as the fuel is burned. The fuel temperature in the tank increases as hot fuel is returned and the overall mass absorbing the heat is reduced.

4. Conclusions

A vehicle-level thermal management aircraft model has been developed in a multidisciplinary modeling and simulation environment using MATLAB/Simulink. The T2T M&S tool enables vehicle level analysis for the aircraft's TMS. The LCA temperature was captured with the interactions with the FTMS, engine, AVS, REPS and HPEAS interaction considered. The newly developed T2T M&S will assist in conceptual design of complex aircraft.

The non-equilibrium interactions between the subsystems is a critical aspect to capture in order to ensure that the vehicle design and controls can maintain operation within the design constraints. The operation of a subsystem outside the design constraints may not be captured with steady-state\equilibrium models. Future studies will focus on TMS design tradeoffs in order to minimize thermal challenges and optimize energy usage. Some possible system trades could be different control architectures for IPP control (constant vs. variable speed), different power sources for the IPP (electric motor driven vs. bleed driven) coupled with component sizing (heat exchangers, IPP or VCS). The T2T M&S tool enables vehicle-level optimization for energy usage and thermal management.

Nomenclature
Acronyms

APTMS	adaptive power and thermal management system
AVS	air vehicle system
DoF	degrees of freedom
ESG	electrical generator
ESG ICC	generator controller
FADEAC	full authority digital engine control
FTMS	fuel thermal management system
HPEAS	high power electrical actuation system
Hyd	hydraulic fluid
HX	heat exchanger
IPP	integrated power package
M&S	modeling and simulation
PTMSC ICC	power and thermal management system controller
PAO	Polyalphaolefin oil
REPS	robust electrical power system
TMS	thermal management system
T2T M&S	tip-to-tail modeling and simulation
VCS	vapor cycle refrigeration system

Parameters

$A =$	area [m^2]
$C=$	coefficient, i
$c_{p_i} =$	constant pressure specific heat, i [kJ/kg/K]
$c_{v_i} =$	constant volume specific heat, i [kJ/kg/K]
$D_h=$	hydraulic diameter [m]
$dt=$	time derivative
$F_i=$	force, i [N]
$f=$	flow efficiency factor
$h_c=$	convective heat transfer coefficient [W/m^2/K]
$h_i =$	specific enthalpy, i [kJ/kg]
$J=$	moment of inertia [kg/m^4]
$k=$	conductance of the free stream [kJ/m/K]
$L=$	characteristic length [m]
$\dot{m}_i=$	mass flow, i [kg/s]
$m_i=$	mass, i [kg]
$MW=$	molecular weight [kg/kmol]
$Ma=$	Mach number
$N_i=$	shaft speed, i [RPM]
$Nu=$	Nusselt number
$\dot{Q}_i =$	heat transferred, i [W]
P_i	pressure of plenum volume, i [kPa]
$Pr =$	Prandtl number
R	ideal gas constant [kJ/kg/K]
R_T	thermal resistance of oil nodes [K/kW]
$Re=$	Reynolds number
$T_i=$	temperature, i [K]
$U_i=$	velocity, i [m/s]
$V=$	volume of plenum volume [m^3]
$\rho_i =$	density, i [kg/m^3]
$\gamma=$	specific heat ratio
$\omega=$	angular velocity [rad/s]
$\dot{\omega}=$	angular acceleration [rad/s^2]
$Weight=$	total weight of aircraft [N]
$\dot{W}$	work rate [kW]

Subscripts

ac	aircraft
atm	atmosphere
actual	actual or real parameter
CL	closed loop turbomachinery
cold	cold flow parameters
comp	parameter of compressor
CV	control valve
D	drag coefficient

D0	constant drag coefficient
D1	drag coefficient for correlation between drag and lift
design	design parameter for turbomachinery
fluid	fluid parameter for either hot, cold, fuel or oil stream
HX	heat exchanger
hot	hot flow parameters
in	inlet parameter of control volume
L0	constant lift coefficient
L	lift
node	specific node parameters
normalized	normalized parameter for turbomachinery
oil	oil parameters
out	outlet parameter of control volume
Power	power turbine in IPP
r	pressure ratio for turbomachinery
shaft	shaft parameters
turb	parameter of turbine
th	throat of orifice

References:

[1] M. Amrhein, J. R. Wells, E. A. Walters, A. F. Matasso, T. R. Erdman, S. M. Iden, P. L. Lamm, A. M. Page, and I. H. Wong, "Integrated Electrical System Model of a More Electric Aircraft Architecture," in *SAE: Power Systems Conference*, Seattle, WA, 2008.

[2] P. Weise, G. Gvozdich, and M. R. Von Spakovsky, "INVENT: Study of the Issues Involved in Integrating a Directed Energy Weapons Subsystem into a High Performance Aircraft System," in *AIAA: Aerospace Sciences Meeting*, Nashville, TN, 2012.

[3] S. P. Mahulikar, H. R. Sonawane, and G. Arvind Rao, Infrared signature studies of aerospace vehicles, *Prog. Aerosp. Sci.*, 43, 218-245, 2007.

[4] J. R. Wells, M. Amrhein, E. A. Walters, S. M. Iden, A. M. Page, P. L. Lamm, and A. F. Matasso, Electrical Accumulator Unit for the Energy Optimized Aircraft, *SAE Int. J. Aerosp.*, 1, 1071-1077, 2008.

[5] W. Lee, D. Choi, and M. Sunwoo, Modelling and simulation of vehicle electric power system, *J. Power Sources*, 109, 58-66, 2002.

[6] H. S. Hamut, I. Dincer, and G. F. Naterer, Analysis and optimization of hybrid electric vehicle thermal management systems, *J. Power Sources*, 247, 643-654, 2014.

[7] M. Wolff, K. McCarthy, G. Russell, J. Zumberge, M. Bodie, and E. Lucas, "Thermal Analysis of an Integrated Aircraft Model," in *AIAA: Aerospace Sciences Meeting*, Orlando, FL, 2010.

[8] K. Mccarthy, M. Amrhein, P. L. Lamm, M. Wolff, K. Yerkes, O. Connell, B. Raczkowski, J. R. Wells, and W. Borger, "INVENT Modeling, Simulation, Analysis and Optimization," in *AIAA: Aerospace Sciences Meeting*, Orlando, FL, 2010.

[9] A. C. Maser, E. Garcia, and D. N. Mavris, "Thermal Management Modeling for Integrated Power Systems in a Transient, Multidisciplinary Environment," in *AIAA/ASME/SAE/ASEE: Joint Propulsion Conference & Exhibit*, Denver, CO, 2009.

[10] F. Uriz Jauregui, B. Remy, A. Degiovanni, and O. Verseux, Model identificaton for temperature extrapolation in aircraft powerplant systems, *Int. J. Therm. Sci.*, 64, 162-177, 2013.

[11] S. M. Eastbourn, 2012, *Modeling and Simulation of a Dynamic Turbofan Engine Using Simulink* (Master thesis), Wright State University, Dayton, OH.

[12] S. M. Eastbourn and R. A. Roberts, "Modeling and Simulation of a Dynamic Turbofan Engine Using Simulink," in *AIAA/ASME/SAE/ASEE: Joint Propulsion Conference & Exhibit*, San Diego, CA, 2011.

[13] R. Chacartegui, D. Sánchez, a. Muñoz, and T. Sánchez, Real time simulation of medium size gas turbines, *Energy Convers. Manag.*, 52, 713-724, 2011.

[14] R. A. Roberts and J. H. Doty, "Implementation of a Non-Equilibrium Exergy Analysis for an Aircraft Thermal Management System," in *AIAA: Aerospace Sciences Meeting*, Nashville, TN, 2012.

[15] F. Incropera and D. P. DeWitt, *Fundamentals of Heat and Mass Transfer*, 4th Ed. New York, NY: John Wiley & Sons, Inc, 2000.

[16] Y. A. Cengel and M. A. Boles, *Thermodynamics: An Engineering Approach*, 6th Ed. New York, NY: McGraw-Hill, 2008.